RSC Advances

ROYAL SOCIETY OF CHEMISTRY

www.rsc.org/advances

Investigation of quinoline-4-carboxylic acid as a highly potent scaffold for the development of alkaline phosphatase inhibitors: Synthesis, SAR analysis and molecular modelling studies

Imtiaz Khan[a†‡], Syed Jawad Ali Shah[b‡], Syeda Abida Ejaz[b‡], Aliya Ibrar[a‡], Shahid Hameed[a,]*,
Joanna Lecka[c,d], Jose Luis Millan[e], Jean Sévigny[c,d] and Jamshed Iqbal[b,]*

[a]*Department of Chemistry, Quaid-i-Azam University, Islamabad-45320, Pakistan*

[b]*Centre for Advanced Drug Research, COMSATS Institute of Information Technology, Abbottabad-22060, Pakistan*

[c]*Département de microbiologie-infectiologie et d'immunologie, Faculté de Médecine, Université Laval, Québec, QC, Canada*

[d]*Centre de Recherche du CHU de Québec – Université Laval, Québec, QC, Canada*

[e]*Sanford Children's Health Research Center, Sanford-Burnham Medical Research Institute, La Jolla, CA 92037*

[†]*Present Address: School of Chemistry, University of Nottingham, University Park, Nottingham, NG7 2RD (UK)*

[‡]*These authors contributed equally.*

The present study is directed towards the development of quinoline-4-carboxylic acid derivatives as potential alkaline phosphatase inhibitors.

1
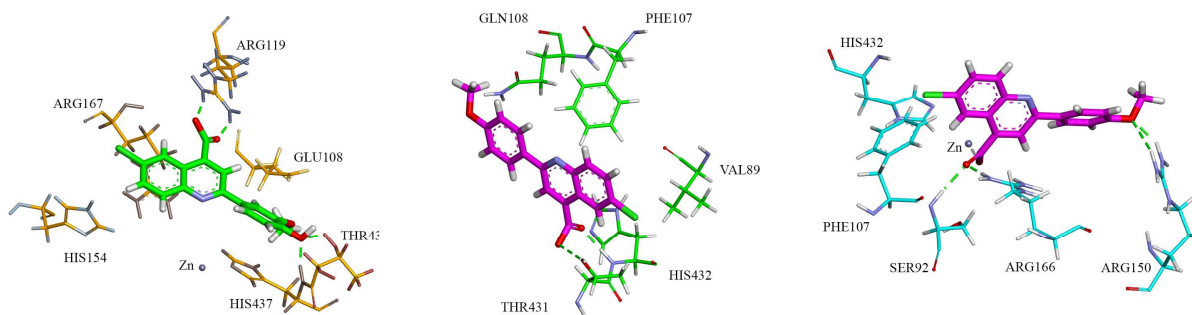
*Corresponding authors. Tel.: +92 51 9064 2133; Fax: +92 51 2241; E-mail: shameed@qau.edu.pk (S. Hameed); +92-992-383591/96; Fax: +92-992-383441. drjamshed@ciit.net.pk (J. Iqbal)

Abstract

The role played by organic chemistry in the pharmaceutical industry continues to be one of the main drives in the drug discovery process. More than ever, the industry demands from organic chemists the development of small molecules, which could be a rich source of biological potential. In this context, a diverse range of quinoline-4-carboxylic acid derivatives has been synthesized and evaluated as potent inhibitors of alkaline phosphatases. The structural build-up

of the synthesized compounds was based on the spectro-analytical data. Most of the tested compounds showed remarkable inhibition of human tissue-nonspecific alkaline phosphatase (*h*-TNAP), tissue specific human intestinal alkaline phosphatase (*h*-IAP) and human placental alkaline phosphatase (*h*-PLAP). Among them, **3j** was identified as a potent inhibitor of *h*-TNAP with an IC$_{50}$ value of 22 ± 1 nM, whereas, **3e** emerged as a lead candidate against *h*-IAP and *h*-PLAP with IC$_{50}$ values of 34 ± 10 and 82 ± 10 nM, respectively. **3a** was a potent inhibitor of human germ cell alkaline phosphatase (*h*-GCAP) with an IC$_{50}$ value of 150 ± 70 nM. The putative binding sites of the most potent inhibitors were inferred from molecular docking simulations using homology models based on the *h*-PLAP structure.

Introduction

Alkaline phosphatases (APs, EC 3.1.3.1) are dimeric enzymes with the ability to dephosphorylate phosphoesters of low molecular mass,[1] and perform phosphotransferase,[2] and protein phosphatase reactions.[3] This isozyme family is comprised of two groups: the tissue-specific alkaline phosphatases which include the intestinal (IAP), placental (PLAP) and germ cell (GCAP) isozymes and the tissue-nonspecific alkaline phosphatase (TNAP), with, each isozyme encoded by different genes.[4,5] Tissue-specific and tissue-nonspecific isozymes can be discriminated by their amino acid sequences and also by their inhibition by inhibitors. TNAP is inhibited by levamisole, histidine and homoarginine but not by L-phenylalanyl-glycyl-glycine (Phe-Gly-Gly), while the reverse is true for the tissue-specific isozymes.[6,7]

Though the expression of TNAP is ubiquitous, it is highly expressed in the developing neural tube, kidney, liver and mineralizing tissues such as cartilage and bone. Its function is intimately associated with mineralization of skeletal and dental tissues, as deficiency in TNAP function in humans and mice leads to a heritable form of rickets/osteomalacia known as hypophosphatasia.[8]

The major function of TNAP in bone tissue is the degradation of extracellular inorganic pyrophosphate (PP_i), a potent inhibitor of calcification, to enable the normal mineralization of skeletal and dental tissues.[9] Thus, inhibitors of TNAP have the potential to be used as a drug to treat disorders of pyrophosphate metabolism such as in generalized arterial calcification of infancy and related rare genetic diseases as well as in chronic kidney disease.[9,10]

On the other hand, placental alkaline phosphatase (PLAP) is expressed in large amounts in the syncytiotrophoblast cells of the placenta from about the eighth week of gestation throughout pregnancy.[11] PLAP was one of the first enzymes recognized as an oncofetal protein expressed in a variety of cancers.[12,13] The germ cells alkaline phosphatase (GCAP) is also expressed in the placenta, although at 1/50 the level of PLAP,[14] but it is expressed in testicular germ cell tumors of the testis, particularly seminomas.[15,16] PLAP and GCAP are often co-expressed in ovarian cancers,[17] and it has been suggested that transformation from normal to malignant trophoblast might be associated with a switch from PLAP to GCAP expression.[18]

Traditionally, levamisole and theophilline have been the only available inhibitors of TNAP with K_i values of 16 and 82 μM, respectively (Figure 1).[19] Recently, however, several groups have screened for and optimized small molecules as efficient and selective inhibitors of AP isozymes.[9,10,20]

Nitrogen is a key component of many natural products and drug molecules. It has been estimated that among all natural products, the average number of nitrogen atoms per molecule is 0.7, while for medicinal drugs, this number rises to 3.0. As an important class of nitrogen-containing heterocycles, quinoline is one of the ubiquitous and privileged structural motifs that occur in bioactive natural products and pharmaceutically active therapeutic agents.[21] Quinoline skeleton is

also one of the key building elements for a large number of natural and synthetic heterocycles which are associated with a range of biological effects such as antimicrobial,[22] anticancer,[23] antimalarial,[24] and antiviral activities.[25] In addition, some natural, semisynthetic and synthetic bioactive molecules based on a quinoline scaffold have been reported to possess multidrug resistance MDR reversal activity when combined with anticancer drug.[26] Numerous quinoline derivatives also display anti-HIV, antiasthmatic, antitumor, P-selectin antagonism, and antioxidant potential.[27]

Keeping in view the literature findings demonstrating the great interest in the research of new bioactive heterocycles and our continued interest in the development of potential AP inhibitors,[28] we have synthesized quinoline-4-carboxylic acid derivatives as a new class of APs inhibitors with enhanced inhibitory potential against human TNAP, IAP, and PLAP. Homology modelling and docking studies were also performed to identify the putative binding modes of the top ranked inhibitors. The results of this study are presented in this paper.

L-Phe   L-Trp   Levamisole   Theophilline
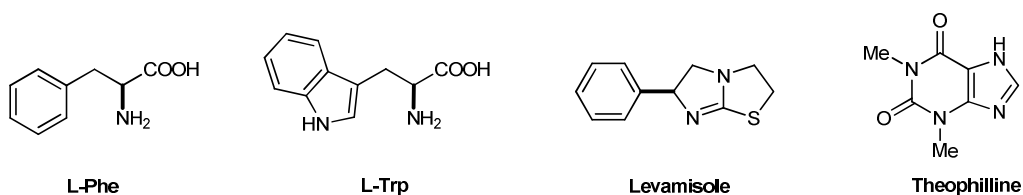
**Fig. 1 Selected examples of AP inhibitors.**

Results and Discussion

Synthesis

Quinoline-4-carboxylic acid derivatives (**3a–j**) were synthesized by the reaction of 5-chloro-isatin **1** with corresponding aryl substituted acetophenones (**2a-j**) in the presence of potassium hydroxide followed by acidification (Scheme 1).[29] Structural modifications were validated by

using a range of substituents (electron–rich and electron–poor) on the aryl ring of acetophenones delivering corresponding condensed products in good yields. Substituents were also tested on variable positions of acetophenones.

Spectroscopic characterization

The formation of compounds **3a–j** was confirmed through ^{1}H NMR spectroscopy where **3a–j** exhibited characteristic signals for carboxylic acid (–COOH) group in the range of 14.50–14.14 ppm along with additional aromatic protons appearing at appropriate chemical shift values. The disappearance of methyl protons of acetophenone also confirmed smooth cyclization. In ^{13}C NMR spectra, distinctive signals in the range of 175.34–155.35 ppm were attributed to the carbonyl carbon of carboxylic acid functional group. The signals for C=N functional group were also found in the appropriate region. The disappearance of the resonances for the carbonyls (ketone and amide) also supported the formation of quinoline-4-carboxylic acids (**3a–j**). The purity of the synthesized compounds was ascertained by elemental analysis.
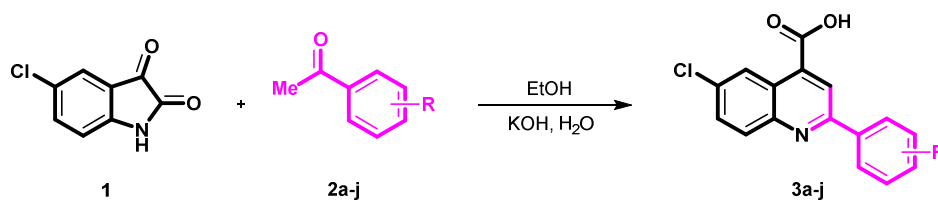
3a: R = 2-Br; **3b**: R = 3-Br; **3c**: R = 3-F; **3d**: R = 3-Me; **3e**: R = 4-OMe; **3f**: R = 4-I;
3g: R = 3-F-4-OMe; **3h**: R = 3-I-4-OMe; **3i**: R = 2,4-diOMe; **3j**: R = 4-OH-3-OMe

Scheme 1 Synthesis of quinoline-4-carboxylic acids (**3a-j**).

Biological activity

Alkaline phosphatase inhibition

The inhibitory activity potential of synthesized compounds **3a-j** against human recombinant APs including TNAP, IAP, PLAP and GCAP was measured using spectrophotometric method.[30] The IC_{50} values were determined for compounds which exhibited over 50% inhibition of either of the above mentioned enzymes and the results are presented in Table 1. Levamisole was used as a positive control for both TNAP and PLAP with an IC_{50} value of 25.2 ± 1.9 and 120 ± 3 µM, respectively. Whereas, L-phenylalanine served as a positive control for both IAP and GCAP with an IC_{50} value of 100 ± 3 and 301 ± 5 µM, respectively.

Interestingly, most of the screened compounds were highly active and inhibited these APs much more efficiently than levamisole and L-phenylalanine. Among the tested compounds, **3j** was identified as a potent inhibitor of TNAP with an IC_{50} value of 22 ± 1 nM, whereas, **3e** emerged as a lead inhibitor of IAP and PLAP with an IC_{50} value of 0.034 ± 0.01 and 0.082 ± 0.01 µM, respectively. Compound **3a** was identified as a potent inhibitor of GCAP with an IC_{50} value of 0.15 ± 0.07 µM.

Structure-activity relationship (SAR) analysis

The inhibitory activity data presented in Table 1 led us to generate an initial structure-activity relationship model where the effect of substitution position on the aryl ring as well as nature of substituent on the activity profile could be explored. As can be seen in Table 1, a number of interesting structure–activity trends could be elucidated from these preliminary screening results. The compound **3a** incorporating an *ortho*-bromo substituent produced a remarkable inhibition potential against TNAP with an IC_{50} value of 0.42 ± 0.02 µM which is ~60-fold higher inhibition as compared to the levamisole (IC_{50} = 25 ± 2 µM). The change of the substituent position from *ortho*- to *meta*- improved inhibition activity upto ~4-fold as compared to compound **3a**. Also, a slight improvement in activity has been noticed when bromo group was replaced by another

7

electronegative fluoro substituent (compound **3c**; IC_{50} = 0.23 ± 0.06 µM). The introduction of a methyl group at *meta*-position of the aryl ring slightly reduced the activity. However, varying the substituent position of an electron-donating group at *para*-position produced comparable results to compounds with *meta*- or *ortho*-substituents. Replacement of methoxy group with a more bulky electron-withdrawing iodo group at *para*-position showed a decreasing trend in activity profile of synthesized compounds. The quinoline analogues with a di-substitution were also active members with enhanced bioactivity. The introduction of polar functional groups like hydroxy at *para*-position along with a methoxy group at *meta*-position like in compound **3j**, resulted in strongest inhibition against TNAP which is ~1145-fold higher potency as compared to levamisole. This enhanced inhibition potential could be attributed to the additional interactions of polar functional groups with the amino acid residues of the target.

The synthesized compounds **3a-j** also showed remarkable inhibitory potency of IAP. The compound **3e** incorporating *para*-methoxy substituent displayed the highest inhibitory activity with an IC_{50} value of 0.03 ± 0.01 µM as compared to the positive control L-phenylalanine (IC_{50} = 100 ± 3 µM). This inhibitory activity strength is 3000-fold higher as compared to L-Phenylalanine which is presumably due to the interactions of amino acid residues with the methoxyl oxygen atom in addition to the other hydrogen bonding contacts making the inhibitor **3e** stabilized in the active pocket of the target. Interestingly, incorporation of a 2-bromo substituent also produced good inhibition character with an IC_{50} value of 0.075 ± 0.001 µM which inhibit enzymatic activity ~1335-fold more potently than standard drug. On moving bromo substituent from *ortho*- to *meta*-position produced diminished results as compared to compounds **3a** and **3e**, but still this potential is ~700-fold higher as compared to L-phenylalanine. Surprisingly, the replacement of bromo substituent with fluoro group or an

electron-donating methyl group led to a significant loss of inhibitory activity (compounds **3c** and **3d**; 43% and 36% inhibition, respectively). Other substitutions such as disubstitution of the aromatic ring also appeared to be tolerated possessing significant inhibitory activity ($IC_{50} = 0.27–0.84$ μM). This observation is mirrored in analogues **3g–3j**, incorporating a combination of electron-rich and electron-deficient functional groups.

Similarly, compounds **3a-j** were also tested for their biological activity against PLAP where compound **3e** was identified as a strong inhibitor with an IC_{50} value of 0.08 ± 0.01 μM as compared to levamisole ($IC_{50} = 120 \pm 3$ μM). This enhanced inhibitory ability of the compound was ~1463-fold stronger as compared to L-phenylalanine (positive) control indicating that the methoxy substituent is necessary for the increased inhibitory activity when placed at *para*-position of the aryl ring. Aromatic ring attached to the quinoline core at 2-position also tolerated bromo, fluoro and methyl groups at *ortho-* and *meta*-position and the inhibitory activity results were promising ($IC_{50} = 0.19–0.32$ μM). We also investigated the effect of the double substitution on the aromatic ring, preparing the 3-F-4-OMe- (**3g**), 3-I-4-OMe- (**3h**), 3,4-diOMe- (**3i**) and 4-OH-3-OMe- (**3j**) analogues. The results revealed that compounds are potent inhibitors of PLAP with strong inhibitory activity depicting IC_{50} values in the range of 0.2-0.7 μM. This inhibition impact was much higher as compared to the levamisole ($IC_{50} = 120 \pm 3$ μM).

Furthermore, when the same compound library was screened against GCAP, only compounds **3a** and **3i** showed extremely high inhibitory potential with an IC_{50} value of 0.15 ± 0.07 and 0.29 ± 0.11 μM, respectively. This inhibition data depicts ~2000- and 1037-fold higher inhibition, respectively for **3a** and **3i,** as compared to the L-phenylalanine ($IC_{50} = 301 \pm 5$ μM). The rest of the analogues showed less than 50% inhibition.

Taken together, the activity results suggest that the variation of the substituent position as well as their nature significantly affect the inhibition potential against TNAP, IAP, and PLAP. These studies also clearly demonstrated that the synthesized compounds have a significant potential to be developed as alkaline phosphatase inhibitors.

Table 1 Alkaline phosphatase inhibition of quinoline-4-carboxylic acid derivatives (3a-j)

| Entry	Substituent (R)	Alkaline phosphatase inhibition			
		h-TNAP	*h*-IAP	*h*-PLAP	*h*-GCAP
		$IC_{50} \pm SEM$ (µM) / % inhibition[a]			
3a	2-Br	0.42 ± 0.02	0.075 ± 0.001	0.32 ± 0.01	0.15 ± 0.07
3b	3-Br	0.11 ± 0.07	0.14 ± 0.01	0.19 ± 0.02	41[a]
3c	3-F	0.23 ± 0.06	43.5[a]	0.19 ± 0.03	45[a]
3d	3-Me	1.1 ± 0.2	36.2[a]	0.28 ± 0.04	47[a]
3e	4-OMe	0.36 ± 0.01	0.03 ± 0.01	0.08 ± 0.01	29[a]
3f	4-I	1.91 ± 0.97	0.21 ± 0.01	1.07 ± 0.21	31[a]
3g	3-F-4-OMe	1.39 ± 0.17	0.49 ± 0.17	0.74 ± 0.12	46[a]
3h	3-I-4-OMe	0.13 ± 0.02	0.84 ± 0.13	0.21 ± 0.03	40[a]
3i	2,4-diOMe	0.12 ± 0.01	0.35 ± 0.01	0.39 ± 0.01	0.29 ± 0.11
3j	4-OH-3-OMe	0.022 ± 0.001	0.27 ± 0.04	0.65 ± 0.09	48[a]
Levamisole		25.2 ± 1.9	—	120 ± 2.5	—
L-Phenylalanine		—	100 ± 3	—	301 ± 5

[a]%inhibition measured at 0.02 mM concentration of inhibitor

(experiments performed in triplicate)

Kinetic studies

Detailed kinetics studies were carried out for compound **3j**, the most active TNAP inhibitor, and it was found to be the uncompetitive inhibitor (Figure 2). Whereas, compound **3e** was found to

be a competitive inhibitor against IAP (Figure 3), and an uncompetitive inhibitor against PLAP (Figure 4).
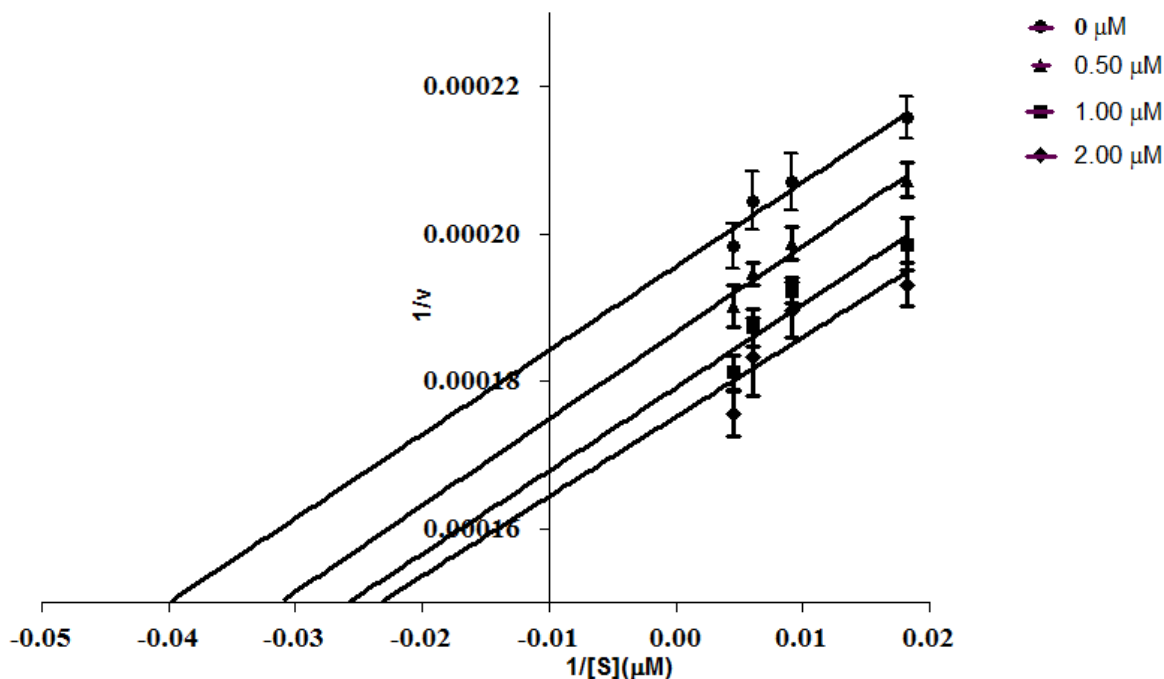
Fig. 2 Double-reciprocal plots of the inhibition kinetics of human tissue non-specific alkaline phosphatase (TNAP) indicating uncompetitive inhibition by compound **3j**. Changes in the initial velocities of the reaction were measured at different concentrations of the inhibitor **3j** using substrate CDP-Star (disodium 2-chloro-5-(4-methoxyspiro[1,2-dioxetane-3,2′-(5-chlorotricyclo[3.3.1.13.7]decan])-4-yl]-1-phenyl phosphate).

11
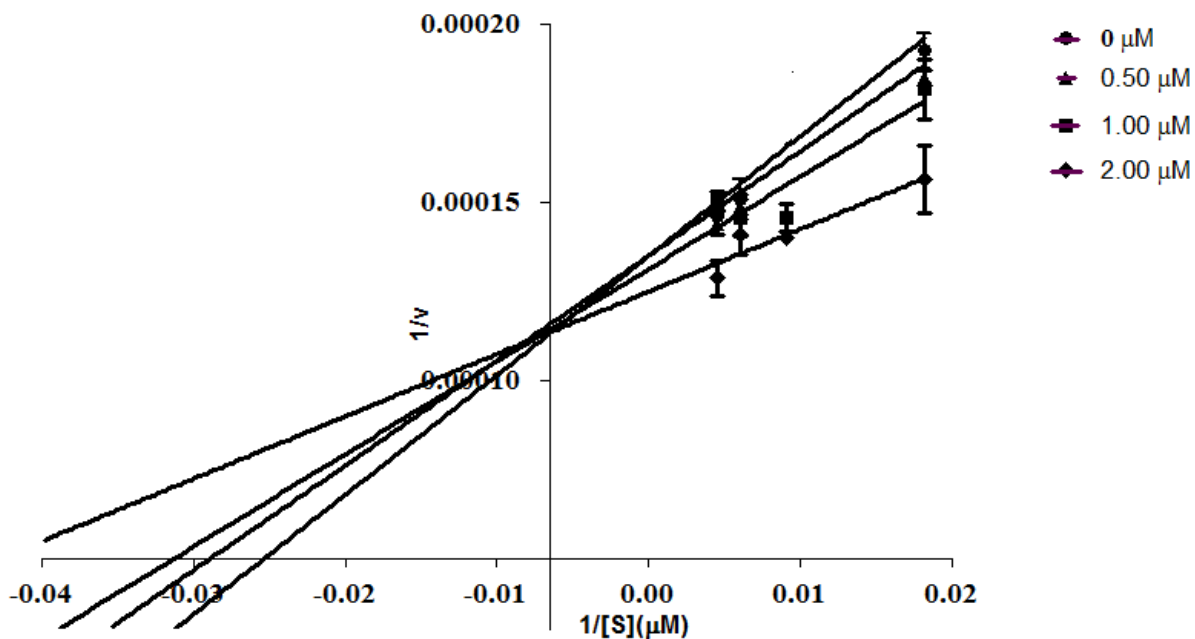
Fig. 3 Double-reciprocal plots of the inhibition kinetics of human tissue specific intestine alkaline phosphatase (IAP) indicating competitive inhibition by compound **3e**. Changes in the initial velocities of the reaction were measured at different concentrations of the inhibitor **3e** using substrate CDP-Star (disodium 2-chloro-5-(4-methoxyspiro[1,2-dioxetane-3,2′-(5-chlorotricyclo[3.3.1.13.7]decan])-4-yl]-1-phenyl phosphate).
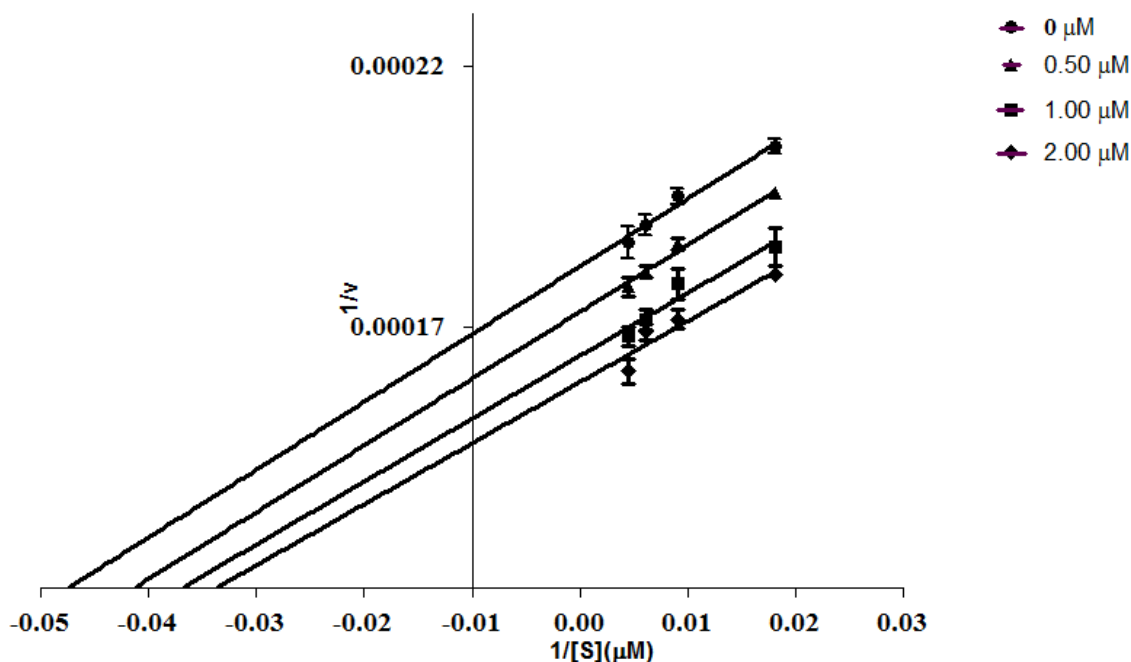
Fig. 4 Double-reciprocal plots of the inhibition kinetics of human tissue specific placental alkaline phosphatase (PLAP) indicating uncompetitive inhibition by compound **3e**. Changes in the initial velocities of the reaction were measured at different concentrations of the inhibitor **3e** using substrate CDP-Star (disodium 2-chloro-5-(4-methoxyspiro[1,2-dioxetane-3,2′-(5-chlorotricyclo[3.3.1.13.7]decan])-4-yl]-1-phenyl phosphate).

Homology modelling of human TNAP and IAP

Comparative modelling of human TNAP and IAP was carried out using Modeller v9.14 *via* Chimera v1.10. Three human placental template sequences (PDB IDs 1ZED, 1EW2 and 3MK0) were identified among the top ten ranking sequences in both cases. In the case of human TNAP, crystal structure (PDB ID 1ZED) was used as template sequence because of its high resolution (1.57 Å) and similarity in amino acid sequence with other identified templates. The template sequence has 90% query coverage and a maximum identity of 58.3% with the target sequence

13

identified. For human IAP, crystal structure (PDB ID 1EW2) with 93% query coverage and 87% sequence identity was used as template. Aligned structure of template and target sequences shows lower RMSD values for both models revealing good quality of alignment. Aligned model of TNAP with template model shows backbone RMSD value of 0.109 Å, while IAP with template model shows backbone RMSD value of 0.121 Å.

Alkaline phosphatases are metal containing enzymes and contain two zinc and one magnesium metal ion in its active site. Modelled protein structures were re-aligned with their respective templates using STAMP tool of VMD v9.1.4,[31] the conservation of amino acid residues was observed. The amino acid Glu429 was found to be substituted with His434 in TNAP and with Ser429 in IAP and imparts specificity to each alkaline phosphatase. All amino acid residues forming the active site and peripheral site are fully conserved in both cases of TNAP and IAP. Figure 5a and 5b shows the conservation of amino acids at active site of TNAP and IAP respectively.

14
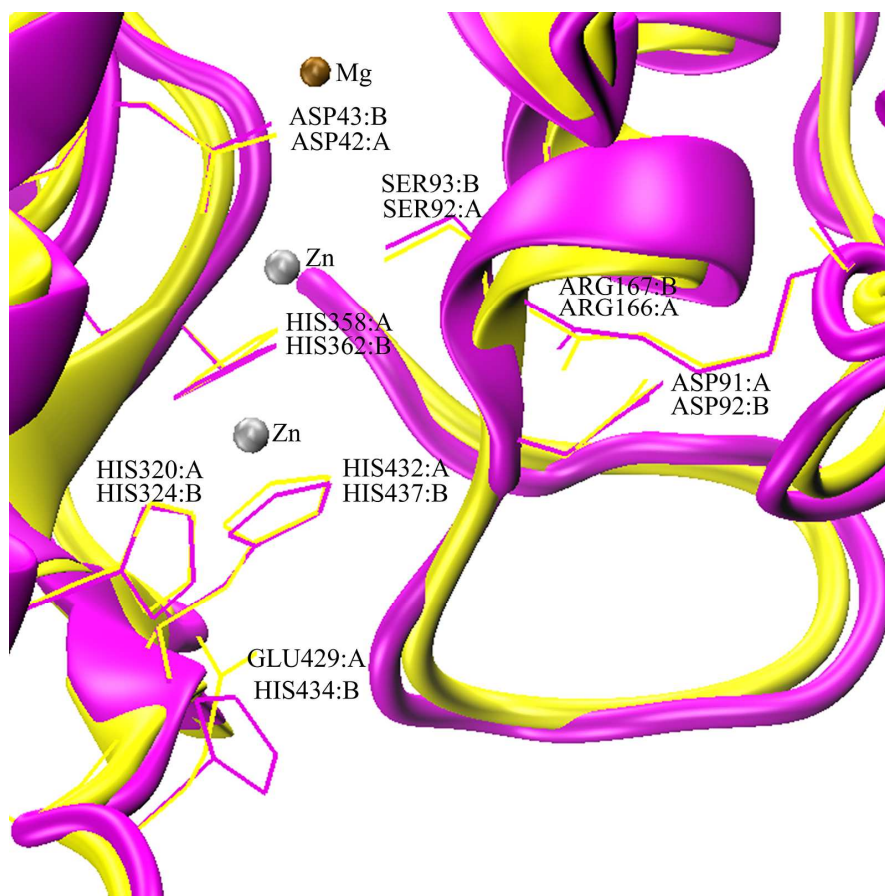
Fig. 5a Comparison of active site of template PLAP crystal structure (yellow, A) with TNAP model (purple, B).
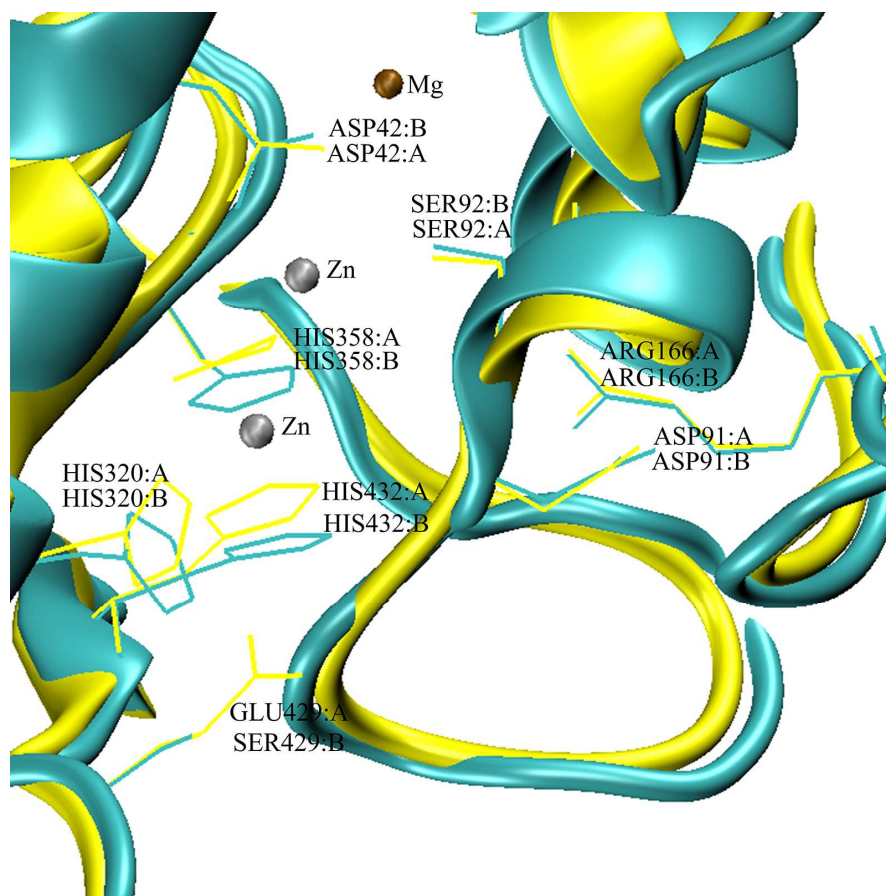
Fig. 5b Comparison of active site of template PLAP crystal structure (yellow, A) with target IAP model (blue, B).

Ramachandran plot[32] of TNAP and IAP models revealed good stereo-chemical quality. 95.2% of the TNAP model residues and 96.9% of IAP residues lied in favored (or core) region of torsion values. 3.1% of TNAP residues and 2.5% of IAP lie in allowed (or generous) regions of torsion values with no amino acid belonging to active site or peripheral site in this region. (See supplementary information for detailed Ramachandran plots of our models with each outlier labelled)

Molecular docking

Active site of tissue specific as well as non-specific alkaline phosphatase contains two Zn ions and one Mg ion. The active site of PLAP is formed by amino acid residues Asp91, Ser92, Gly93, Arg166 and Glu429. Additionally, the amino acid His430 and His432 forms hydrogen bonds with negatively charged moiety such as phosphoryl oxy-moiety.[33] The corresponding active site amino acids of TNAP includes; Asp92, Ser93, Ala94, Arg167, His434, His435 and His437.

Previously, molecular docking studies of standard uncompetitive inhibitors in human TNAP revealed amino acids Glu108, Gly109, Tyr371 and His434 as major interacting amino acids. While in case of human PLAP the equivalent amino acids are Phe107, Gln108, Tyr367 and Glu429.[19] The human IAP contains same amino acids as that of human PLAP with a substitution of Ser429 instead of Glu429.

Compound **3j** was the most potent inhibitor of human TNAP. Binding mode of compound **3j** was similar to that of PLAP. It was found to have interaction with amino acid His437 through a hydrogen bond. Amino acid His437 in TNAP is similar to His432 in PLAP, where it forms hydrogen bonding with phosphoryl oxy-moiety during substrate hydrolysis. Due to lack of positively charged group, interaction of compound **3j** with Glu108 was not observed. Amino acid Arg167 forms interaction with chloride atom of the compound. Arg167 is the same amino acid as Arg166 in PLAP. Additionally, Arg119 was observed to form hydrogen bonding interaction with carboxyl moiety of our compound. Interaction of compound **3j** with TNAP can be seen in Fig. 6.

Compound **3e** was identified to have different modes of interaction with PLAP and IAP respectively. Due to the lack of positively charged group in compound **3e**, interaction with Glu429 was not observed. It was found that compound **3e** interacts with residues His432 and Gln108. Interaction of compound **3e** with His432 may prevents the binding of His432 with

17

phosphoryl oxy-moiety formed during substrate hydrolysis and cause uncompetitive inhibition of PLAP. Fig. 6 shows the interaction of compound **3e** inside human PLAP enzyme.

Compound **3e** in human IAP was the most potent inhibitor and the enzyme kinetic studies revealed competitive mode of inhibition unlike those found for TNAP or PLAP. The possible explanation of the competitive inhibition can be deduced from the fact that compound **3e** forms a hydrogen bonding interaction with catalytic amino acid Ser92 and also binds zinc metal ion. Additionally, compound **3e** was also found to have a hydrogen bonding contact with active site amino acid Arg166. As mentioned previously, alkaline phosphatase are class of enzymes belonging to serine hydrolases and thus, amino acid Ser92 plays an important role in hydrolysis of phosphomonoesters through catalytic activation by zinc ion,[34] thus interaction of compound **3e** with zinc and amino acid Ser92 decreases its interaction with substrate and therefor, causes competitive inhibition. Interaction of compound **3e** inside the active pocket of human IAP can be seen in Fig. 6.
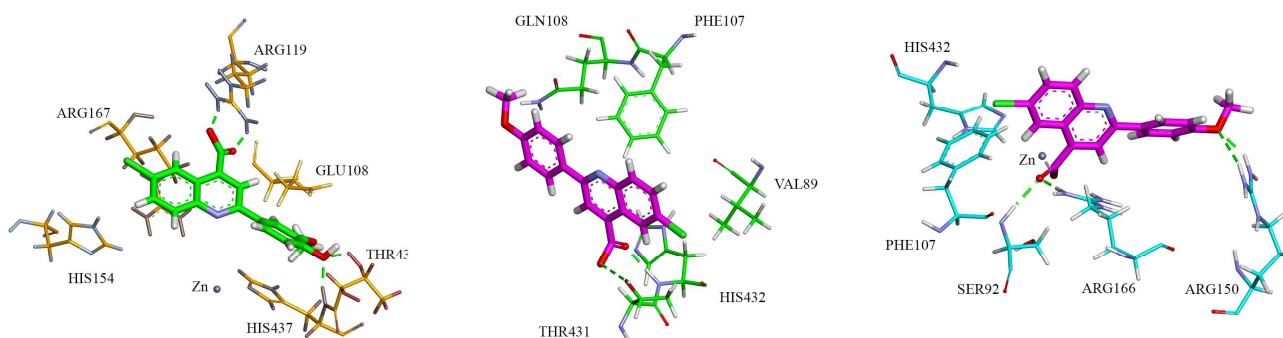
Fig. 6 Putative binding mode of compound **3j** (colored green) inside TNAP model (colored brown) and compound **3e** (colored magenta) inside the crystal structure of PLAP (colored green)

and inside the IAP model (colored cyan). Hydrogen bonding are shown in green colored dashed lines.

HYDE assessment and visual affinity

Hyde assessment was performed for the compounds **3j** inside TNAP, and **3e** inside the active pocket of PLAP and IAP. FlexX docking score and binding free energy ΔG were determined as shown in Table 2.

Table 2 Docking score and HYDE score of compounds 3e and 3j

Compound	Receptor	FlexX Score of the top ranking pose	Binding Free Energy ΔG (KJmol^{-1})	Poser Rank
3j	TNAP	-26.27	-21	26
3e	PLAP	-20.19	-12	08
3e	IAP	-24.50	-12	07

Conclusions

In summary, we have explored a new class of tissue-nonspecific and tissue-specific AP inhibitors based on the quinoline template. Almost, all members of the compound library exhibited strong and effective inhibitory activity. Among them, **3j** was identified as the most potent inhibitor against TNAP with an IC$_{50}$ value of 0.022 ± 0.001 μM, whereas, **3e** emerged as a lead candidate against IAP and PLAP activities with an IC$_{50}$ value of 0.03 ± 0.01 and 0.08 ± 0.01 μM, respectively. Against GCAP, **3a** was a ~2000-fold stronger inhibitor than L-phenylalanine with an IC$_{50}$ value of 0.15 ± 0.07 μM. Structure-activity relationship studies demonstrated that the presence of electron-donating and electron-withdrawing substituents as well as their substitution position imparts a marked effect on the inhibition profile. The docking study results for the tested compounds were explanatory of the enzyme inhibitory assay results, where the observed binding

interactions poses clarified the binding modes and binding energy scores of these derivatives. Finally, based on all the above-mentioned investigations, this novel class of alkaline phosphatase inhibitors described here provides an opportunity for further medicinal chemistry efforts to aid in the design of second generation compounds.

Experimental

Materials and methods

Unless otherwise noted, all materials were obtained from commercial suppliers (Aldrich and Merck companies) and used without further purification. Thin layer chromatography (TLC) was performed on Merck DF-Alufoilien 60F$_{254}$ 0.2 mm precoated plates. Product spots were visualized under UV light at 254 and 365 nm. Melting points were recorded on a Stuart melting point apparatus (SMP3) and are uncorrected. Infra-red (IR) spectra were recorded on FTS 3000 MX, Bio-Rad Merlin (Excalibur model) spectrophotometer. ^{1}H NMR spectra were recorded on a Bruker Avance (300 MHz) spectrometer. Chemical shifts (δ) are quoted in parts per million (ppm) downfield of tetramethylsilane, using residual solvent as internal standard (DMSO-d_6 at 2.50 ppm). Abbreviations used in the description of resonances are: s (singlet), d (doublet), dd (doublet of doublet), t (triplet), q (quartet), m (multiplet), Ar (aromatic). Proton-decoupled ^{13}C NMR spectra were recorded on a Bruker Avance (75 MHz) spectrometer using deuterated solvent as internal standard (DMSO-d_6 at 39.52 ppm). The elemental analysis was performed on Leco CHNS-932 Elemental Analyzer, Leco Corporation (USA).

Synthesis

Preparation of quinoline-4-carboxylic acids (3a–j): General procedure

Into an oven-dried round-bottomed flask fitted with a reflux condenser was added 5-chloroisatin (1.0 mmol) in ethanol (5 mL). An ethanolic solution of appropriate acetophenone (1.1 mmol)

was added into the flask followed by the gradual addition of KOH (3.0 mmol). The reaction mixture was refluxed for 24 h. It was then cooled to room temperature, and ethanol was removed under reduced pressure. The residue was acidified with 2M aqueous hydrochloric acid until the pH becomes 2.0. The precipitated solid was collected by filtration, washed with brine and dried under vacuum. The crude product was purified by recrystallization from ethanol to afford the corresponding quinolone-4-carboxylic acid derivatives (**3a-j**).[29] The data obtained for compound **3e** was consistent with the literature.[29]

2-(2-Bromophenyl)-6-chloroquinoline-4-carboxylic acid (3a)

The general experimental procedure described above afforded **3a** as an off-white solid. Yield: 68%; m.p 264-265 °C; R_f: 0.44 (10% MeOH/CHCl$_3$); IR (ATR, cm^{-1}): 2533 (COOH), 1716 (C=O), 1584 (C=N), 1539, 1494 (C=C); ^{1}H NMR (300 MHz, DMSO-d_6): δ 14.35 (s, 1H, COOH), 8.87 (d, 1H, J = 2.4 Hz, Ar-H), 8.22 (s, 1H, Ar-H), 8.15 (d, 1H, J = 9.0 Hz, Ar-H), 7.87 (dd, 1H, J = 2.4, 2.4 Hz, Ar-H), 7.79 (dd, 1H, J = 1.2, 0.9 Hz, Ar-H), 7.67 (dd, 1H, J = 1.8, 1.8 Hz, Ar-H), 7.57-7.52 (m, 1H, Ar-H), 7.47-7.42 (m, 1H, Ar-H); ^{13}C NMR (75 MHz, DMSO-d_6): δ 167.26, 158.76, 147.20, 140.38, 135.16, 133.57, 132.26, 132.16, 131.47, 131.16, 128.52, 125.00, 124.89, 124.71, 121.47. Analysis Calcd. for C$_{16}$H$_9$BrClNO$_2$ (360.95): C, 53.00; H, 2.50; N, 3.86. Found: C, 52.88; H, 2.64; N, 3.67.

2-(3-Bromophenyl)-6-chloroquinoline-4-carboxylic acid (3b)

The general experimental procedure described above afforded **3b** as an off-white solid. Yield: 70%; m.p 243-244 °C; R_f: 0.42 (10% MeOH/CHCl$_3$); IR (ATR, cm^{-1}): 2520 (COOH), 1716 (C=O), 1589 (C=N), 1547, 1499 (C=C); ^{1}H NMR (300 MHz, DMSO-d_6): δ 8.73 (d, 1H, J = 2.1 Hz, Ar-H), 8.44 (s, 1H, Ar-H), 8.39 (d, 1H, J = 1.8 Hz, Ar-H), 8.19 (d, 1H, J = 7.8 Hz, Ar-H), 8.10 (d, 1H, J = 9.0 Hz, Ar-H), 7.79 (dd, 1H, J = 2.4, 2.4 Hz, Ar-H), 7.70-7.67 (m, 1H, Ar-H),

7.48 (t, 1H, J = 7.8 Hz, Ar-H); ^{13}C NMR (75 MHz, DMSO-d_6): δ 167.68, 154.96, 147.16, 140.25, 138.21, 133.18, 132.96, 132.21, 131.51, 131.06, 130.10, 126.64, 125.04, 125.00, 122.96, 120.56. Analysis Calcd. for $C_{16}H_9BrClNO_2$ (360.95): C, 53.00; H, 2.50; N, 3.86. Found: C, 52.81; H, 2.37; N, 3.72.

6-Chloro-2-(3-fluorophenyl)quinoline-4-carboxylic acid (3c)

The general experimental procedure described above afforded **3c** as an off-white solid. Yield: 64%; m.p 233-234 °C; R_f: 0.41 (10% MeOH/CHCl$_3$); IR (ATR, cm^{-1}): 3221 (COOH), 1715 (C=O), 1584 (C=N), 1541, 1497 (C=C); ^{1}H NMR (300 MHz, DMSO-d_6): δ 14.18 (s, 1H, COOH), 8.72 (d, 1H, J = 2.3 Hz, Ar-H), 8.42 (s, 1H, Ar-H), 8.39 (d, 1H, J = 1.8 Hz, Ar-H), 8.21 (d, 1H, J = 7.8 Hz, Ar-H), 8.12 (d, 1H, J = 9.0 Hz, Ar-H), 7.70 (dd, 1H, J = 2.4, 2.4 Hz, Ar-H), 7.69-7.66 (m, 1H, Ar-H), 7.45 (t, 1H, J = 7.8 Hz, Ar-H); ^{13}C NMR (75 MHz, DMSO-d_6): δ 175.34, 168.12, 155.13, 152.78, 150.56, 147.91, 147.79, 146.98, 135.66, 132.08, 132.00, 131.36, 130.44, 129.95, 126.92, 126.02, 124.07, 114.46, 114.20. Analysis Calcd. for $C_{16}H_9ClFNO_2$ (301.03): C, 63.70; H, 3.01; N, 4.64. Found: C, 63.54; H, 2.97; N, 4.52.

6-Chloro-2-*m*-tolylquinoline-4-carboxylic acid (3d)

The general experimental procedure described above afforded **3d** as a yellow solid. Yield: 63%; m.p 225-226 °C; R_f: 0.42 (10% MeOH/CHCl$_3$); IR (ATR, cm^{-1}): 3303 (COOH), 2926, 2842 (CH$_3$), 1680 (C=O), 1612 (C=N), 1544, 1510 (C=C); ^{1}H NMR (300 MHz, DMSO-d_6): δ 8.90 (d, 1H, J = 2.4 Hz, Ar-H), 8.19 (s, 1H, Ar-H), 8.16 (bs, 2H, Ar-H), 7.92 (d, 1H, J = 9.0 Hz, Ar-H), 7.64 (dd, 1H, J = 2.4, 2.4 Hz, Ar-H), 7.12 (d, 2H, J = 8.4 Hz, Ar-H), 2.53 (s, 3H, CH$_3$); ^{13}C NMR (75 MHz, DMSO-d_6): δ 174.69, 168.11, 160.23, 156.38, 147.62, 147.20, 131.56, 131.38, 130.01, 128.97, 128.54, 126.90, 125.53, 121.72, 117.69, 114.21, 28.70. Analysis Calcd. for $C_{17}H_{12}ClNO_2$: C, 68.58; H, 4.06; N, 4.70. Found: C, 68.49; H, 3.91; N, 4.61.

6-Chloro-2-(4-iodophenyl)quinoline-4-carboxylic acid (3f)

The general experimental procedure described above afforded **3f** as an off-white solid. Yield: 70%; m.p 260-261 °C; R_f: 0.43 (10% MeOH/CHCl$_3$); IR (ATR, cm^{-1}): 3206 (COOH), 1716 (C=O), 1613 (C=N), 1557, 1538 (C=C); ^{1}H NMR (300 MHz, DMSO-d_6): δ 8.98 (d, 1H, J = 1.8 Hz, Ar-H), 8.26 (s, 1H, Ar-H), 8.12 (d, 2H, J = 8.4 Hz, Ar-H), 7.98 (d, 1H, J = 9.0 Hz, Ar-H), 7.67-7.63 (m, 3H, Ar-H); ^{13}C NMR (75 MHz, DMSO-d_6): δ 155.35, 147.12, 138.07, 132.17, 131.49, 130.88, 130.04, 129.47, 126.90, 126.21, 123.72, 118.43. Analysis Calcd. for C$_{16}$H$_9$ClINO$_2$ (408.94): C, 46.92; H, 2.21; N, 3.42. Found: C, 46.81; H, 2.12; N, 3.34.

6-Chloro-2-(3-fluoro-4-methoxyphenyl)quinoline-4-carboxylic acid (3g)

The general experimental procedure described above afforded **3g** as an off-white solid. Yield: 66%; m.p 298-299 °C; R_f: 0.41 (10% MeOH/CHCl$_3$); IR (ATR, cm^{-1}): 3343 (COOH), 2945, 2838 (CH$_3$), 1693 (C=O), 1616 (C=N), 1542, 1517 (C=C); ^{1}H NMR (300 MHz, DMSO-d_6): δ 14.14 (s, 1H, COOH), 8.74 (d, 1H, J = 2.1 Hz, Ar-H), 8.50 (s, 1H, Ar-H), 8.18-8.10 (m, 3H, Ar-H), 7.86-7.83 (m, 1H, Ar-H), 7.36-7.31 (m, 1H, Ar-H), 3.94 (s, 3H, OCH$_3$); ^{13}C NMR (75 MHz, DMSO-d_6): δ 175.29, 169.32, 155.14, 153.78, 150.56, 148.93, 148.79, 148.57, 147.08, 132.08, 132.00, 131.36, 130.44, 129.93, 126.90, 126.00, 124.07, 117.80, 114.72, 114.47, 114.20, 56.51. Analysis Calcd. for C$_{17}$H$_{11}$ClFNO$_3$ (331.04): C, 61.55; H, 3.34; N, 4.22. Found: C, 61.32; H, 3.39; N, 4.09.

6-Chloro-2-(3-iodo-4-methoxyphenyl)quinoline-4-carboxylic acid (3h)

The general experimental procedure described above afforded **3h** as a light yellow solid. Yield: 73%; m.p 251-252 °C; R_f: 0.39 (10% MeOH/CHCl$_3$); IR (ATR, cm^{-1}): 3271 (COOH), 2926, 2838 (CH$_3$), 1686 (C=O), 1583 (C=N), 1557, 1538 (C=C); ^{1}H NMR (300 MHz, DMSO-d_6): δ 14.18 (s, 1H, COOH), 8.95 (d, 1H, J = 2.1 Hz, Ar-H), 8.65 (d, 1H, J = 1.5 Hz), 8.17 (s, 2H, Ar-

H), 7.99 (d, 1H, J = 9.0 Hz, Ar-H), 7.66 (dd, 1H, J = 2.1, 2.1 Hz, Ar-H), 7.11 (d, 1H, J = 8.7 Hz,

Ar-H), 3.90 (s, 3H, OCH$_3$); ^{13}C NMR (75 MHz, DMSO-d_6): δ 167.56, 153.91, 147.23, 140.47,

138.65, 133.49, 132.21, 132.11, 131.51, 131.08, 130.04, 126.84, 125.62, 125.01, 122.76, 120.56,

56.45. Analysis Calcd. for C$_{17}$H$_{11}$ClNO$_3$ (438.95): C, 46.44; H, 2.52; N, 3.19. Found: C, 46.31;

H, 2.65; N, 3.27.

6-Chloro-2-(2,4-dimethoxyphenyl)quinoline-4-carboxylic acid (3i)

The general experimental procedure described above afforded **3i** as a light orange solid. Yield:

79%; m.p 239-240 °C; R$_f$: 0.47 (10% MeOH/CHCl$_3$); IR (ATR, cm^{-1}): 3478 (OH), 3265

(COOH), 2938, 2840 (CH$_3$), 1726 (C=O), 1619 (C=N), 1583, 1542 (C=C); ^{1}H NMR (300 MHz,

DMSO-d_6): δ 14.50 (s, 1H, COOH), 9.65 (s, 1H, OH), 8.70 (d, 1H, J = 2.4 Hz, Ar-H), 8.44 (s,

1H, Ar-H), 8.04-7.99 (m, 2H, Ar-H), 7.82-7.74 (m, 1H, Ar-H), 6.55-6.44 (m, 2H, Ar-H), 3.80 (s,

3H, OCH$_3$), 3.75 (s, 3H, OCH$_3$); ^{13}C NMR (75 MHz, DMSO-d_6): δ 167.33, 156.87, 149.60,

147.54, 140.76, 136.21, 132.66, 132.09, 131.91, 131.76, 129.10, 125.34, 125.13, 122.94, 119.43,

111.34, 56.38, 54.65. Analysis Calcd. for C$_{17}$H$_{12}$ClNO$_4$ (343.06): C, 62.89; H, 4.10; N, 4.07.

Found: C, 62.78; H, 3.98; N, 4.11.

6-Chloro-2-(4-hydroxy-3-methoxyphenyl)quinoline-4-carboxylic acid (3j)

The general experimental procedure described above afforded **3j** as a yellow solid. Yield: 77%;

m.p 249-250 °C; R$_f$: 0.46 (10% MeOH/CHCl$_3$); IR (ATR, cm^{-1}): 3478 (OH), 3273 (COOH),

2945, 2840 (CH$_3$), 1690 (C=O), 1613 (C=N), 1585, 1522 (C=C); ^{1}H NMR (300 MHz, DMSO-

d_6): δ 9.60 (s, 1H, OH), 8.71 (d, 1H, J = 2.4 Hz, Ar-H), 8.45 (s, 1H, Ar-H), 8.10 (d, 1H, J = 9.0

Hz, Ar-H), 7.87 (d, 1H, J = 1.8 Hz, Ar-H), 7.81-7.72 (m, 2H, Ar-H), 6.95 (d, 1H, J = 8.4 Hz, Ar-

H), 3.92 (s, 3H, OCH$_3$); ^{13}C NMR (75 MHz, DMSO-d_6): δ 167.81, 156.73, 149.62, 148.56,

147.34, 131.98, 130.85, 129.31, 124.84, 124.34, 121.22, 120.42, 116.25, 111.20, 56.19. Analysis

Calcd. for $C_{17}H_{12}ClNO_4$ (329.05): C, 61.92; H, 3.67; N, 4.25. Found: C, 61.99; H, 3.53; N, 4.14.

Biological protocol

Cell transfection with human alkaline phosphatases

COS-7 cells were transfected in 10-cm plates with Lipofectamine, as reported previously,[35] using

plasmids expressing human APs (TNAP, PLAP, IAP, and GCAP). The plasmids encoding human

TNAP, PLAP and IAP have been described in published report,[36,37] and the plasmid expressing

human GCAP was purchased from OriGene Technology Inc. (OriGene, Rockville MD). In short,

confluent cells were incubated for 5 h at 37 °C in DMEM/F-12 in the absence of fetal bovine

serum and with 6 µg of plasmid DNA and 24 µL of Lipofectamine reagent. The transfection was

stopped by adding the same volume of DMEM/F-12 containing 20% FBS and the cells were

harvested 48–72 h later.

Preparation of protein extracts

Preparation of protein extracts was done as reported previously.[35] Briefly, transfected cells were

washed three times at 4 °C, with Tris–saline buffer, collected by scraping in the harvesting buffer

(95 mM NaCl, 0.1 mM PMSF, and 45 mM Tris buffer, pH 7.5) and washed twice by

centrifugation at 300×g for 5 min at 4 °C. Subsequently, cells were resuspended in the harvesting

buffer containing 10 µg/mL aprotinin and sonicated. Nuclear and cellular debris were discarded

by 10 min centrifugation (300×g at 4 °C). Glycerol was added to the resulting supernatant at a

final concentration of 7.5%. Samples were kept at −80 °C until used. Protein concentration was

estimated using Bradford microplate assay and bovine serum albumin was used as a standard.[36]

Alkaline phosphatase inhibition assay

A chemiluminescent substrate, CDP-star with or without tested inhibitors, was used for the determination of AP activity. For this the recombinant form of the following enzymes expressed in COS-7 cells as before[38] were prepared: TNAP, IAP, PLAP and GCAP.[10,19, 20] The conditions for the assay were optimized with the slight modifications in previously used spectrophotometric method.[30] The assay buffer which contained 8 M DEA (pH 9.8), 2.5 mM $MgCl_2$ and 0.05 mM $ZnCl_2$ was used. Initial screening was performed at a concentration of 0.2 mM of the tested compounds. The total volume of 50 μL contained 10 μL of each tested compound (0.02 mM (initial concentration) with final DMSO 1% (v/v)), followed by the addition of 20 μL of h-TNAP (from 2.29μg/mL enzyme in assay buffer), 20 μL of h-IAP (from 2.84 μg/mLenzyme in assay buffer), 20 μL of h-PLAP (from 3.0 μg/mL enzyme in assay buffer) and 20 μL of h-GCALP (2.92 μg/mL enzyme in assay buffer), in respective enzyme assay. The mixture was pre-incubated for 5-7 minutes at 37 °C and luminescence was measured as pre-read using microplate reader (BioTek FLx800, Instruments, Inc. USA). Then, in the respective enzymatic assay, 20 μL of CDP-star (final concentration of 110 μM) was added to initiate the reaction and the assay mixture was incubated again for 15 min at 37 °C. The change in the luminescence was measured as after-read. The activity of each compound was compared with total activity control (without any inhibitor). Levamisole (0.2 mM per well) was used as a positive control for both the TNAP and PLAP isozymes. While, L-phenylalanine (0.4 mM per well) was used as a positive control for IAP. For potentially active compounds, full concentration inhibition curves were produced. The compounds which exhibited over 50% inhibition of either of the above mentioned enzymes were further evaluated for determination of IC_{50} values. For this purpose 6 to 8 serial dilutions of each compound were prepared in assay buffer and their dose response curves were obtained by assaying each inhibitor concentration against all APs using the above mentioned reaction

conditions. All experiments were repeated in triplicate. The Cheng Prusoff equation was used to calculate the IC_{50} values, determined by the non-linear curve fitting program PRISM 5.0 (GraphPad, San Diego, California, USA).

Kinetics study

Michaelis-Menten kinetic experiments were used to determine the enzyme inhibition interaction mode of the quinoline-4-carboxylic acid with the binding site of *h*-TNAP, *h*- IAP and *h*-PLAP. For this purpose, the initial rates of the enzyme inhibition at four different substrate concentrations (55 µM, 110 µM, 165 µM and 220 µM) in the absence and in the presence of four different concentrations (0 µM, 0.50 µM, 1.00 µM and 2.00 µM) of the selected representative inhibitor **3j** against *h*-TNAP and **3e** against IAP and PLAP were measured. The Lineweaver-Burk plot for different concentrations of **3j** was linear at the Y axis with the plot for the uninhibited enzyme. The Lineweaver-Burk plot for different concentrations of **3e** was linear in case of *h*-PLAP and was intersected in case of *h*-IAP, at the y-axis with the plot for the uninhibited enzyme.

Homology modelling of TNAP and IAP

Homology modelling of human derived tissue non-specific alkaline phosphatase was carried out using Modeller v9.14[39] *via* Chimera v1.10.[40] Target sequence of TNAP (Uniprot ID P05186) was searched in NCBI protein database and was fetched into Chimera. Template sequences for homology modelling were identified by using BLAST (Basic Local Allignment Search Tool) protein database.[41] Three human template sequences (PDB ID: 1ZED, 1EW2 and 3MK0) were identified among top ten sequences. Using Needleman Wunsch method embedded in Chimerav1.10 template sequence of human TNAP (Uniprot ID P05168) was added to the template sequence (PDB ID 1ZED). Comparative homology modelling of the template sequence

was performed by running Modeller v9.14[39] *via* Chimera v1.10.[40] The template and the model

structure was re-aligned by using STAMP (Structural Alignment for Multiple Proteins) tool of

VMD v9.1.4.[31] The quality of model was evaluated and the conservation of amino acid residues,

especially at the active site was evaluated. Different parameters of model quality such as RMSD

and percentage identity was also determined for the modelled proteins. To further evaluate the

quality of protein, Ramachandran plot was generated using RAMPAGE[32] Ramachandran plot

utility of Cambridge University.

Homology model of the human IAP was also carried out using the same methodology as

described above. The target sequence of human IAP was searched in NCBI protein database,

Uniprot ID P09923 was identified. Using BLAST protein utility crystal structures of human

PLAP were identified as the top ranking templates. Human placental alkaline phoshatase PDB

ID 1EW2 was used, models generated were subjected to same set of evaluations as used above

for human TNAP model.

Binding mode analysis

Preparation of receptors and ligands for docking

Crystal Structure of human PLAP (PDB ID 1ZED) was downloaded from RCSB Protein Data

Bank. For TNAP and IAP, modelled protein structures were used. Prior to docking, the

modelled protein structures of TNAP and IAP were prepared by using Dock Prep utility of

Chimera v1.10.[40] which includes addition of hydrogen atoms and Gasteiger charges, energy

minimization and completing the incomplete side chains using Dunbrack rotamer library. A net

charge of +2 was added to Zn and Mg ions and the modelled structures were then saved in pdb

file format.

Chemical structures of compounds **3e** and **3j** were drawn using ACD/ChemSketch[42] and 3D

optimized. Using ANTECHAMBER[43] utility of Chimera v.1.10. Gasteiger charges were added

and the structures were energy minimized through 100 steepest descent and conjugate steps, with

each step size of 0.02 Å. Compound structures were then saved as mol2 file format.

Molecular docking

Molecular docking of the most potent compounds **3j** and **3e** was carried out using LeadIT from

BioSolveIT, GmbH Germany.[44] Using Load or Prepare Receptor utility of the LeadIT software

the receptor was loaded and the metal ions were selected as part of the receptor. Active site of

the receptor for docking studies was identified as the amino acid residues in 7.5 Å radius around

phosphate ion. Default values of amino acids flips, water handling and metal co-ordinates were

selected.

Using FlexX utility of LeadIT, docking of compounds was performed. Default docking

parameters were selected and top 50 highest scoring docked positions were kept and analyzed

further. Visualization of poses was performed using Discovery studio visualizer v4.0.[45]

Using HYDE visual affinity[46] program of LeadIT the binding affinity of the docked poses were

evaluated. The HYDE scoring is a function of two parameters i.e. hydrogen bond affinity and

dehydration energy. Binding free energy i.e. ΔG was determined for each pose and noted down.

Poses with lowest ΔG values were considered as the most stable pose with highest affinity for

interaction with our receptor.

Acknowledgments

Supplementary material

The supporting information related to this article can be found with the online version of the paper.

References

1. R. B. McComb, G. N. Bowers and S. Posen, Alkaline phosphatase. New York: Plenum Press; 1979.

2. R. A. Stinson, J. L. McPhee and H. B. Collier, *Biochim. Biophys. Acta*, 1987, **913**, 272-278.

3. J. R. Chan and R. A. Stinson, *J. Biol. Chem.*, 1986, **261**, 7635-7639.

4. M. Lanier, E. Sergienko, A. M. Simao, Y. Su, T. Chung, J. L. Millan and J. R. Cashman, *Bioorg. Med. Chem.*, 2009, **18**, 573-579.

5. E. A. Sergienko and J. L. Millan, *Nat. Protoc.*, 2010, **5**, 1431-1439.

6. van Belle, *Clin. Chem.*, 1978, **22**, 972-976.

7. R. A. Mulivor, L.I. Plotkin and H. Harris, *Ann. Hum. Genet.*, 1978, **42**, 1-13.

8. J. L. Millán, Mammalian Alkaline Phosphatases: From Biology to Applications in Medicine and Biotechnology; Wiley-VCH: Weinheim, Germany, 2006.

9. S. Sidique, R. Ardecky, Y. Su, S. Narisawa, B. Brown, J. L. Millán, E. Sergienko and N. D. P. Cosford, *Bioorg. Med. Chem. Lett.*, 2009, **19**, 222-225.

10. (a) S. Narisawa, D. Harmey, M. C. Yadav, W. C. O'Neill, M. F. Hoylaerts and J. L. Millán, *J. Bone Miner. Res.*, 2007, **22**(11), 1700-1710; (b) R. Dahl, E. A. Sergienko, Y. Su, Y. S. Mostofi, L. Yang, A. M. Simão, S. Narisawa, B. Brown, A. Mangravita-Novo, M. Vicchiarelli, L. H. Smith, W. C. O'Neill, J. L. Millán and N. D. Cosford, *J. Med. Chem.*, 2009, **52**(21), 6919-6925; (c) L. Li, L. Chang, S. Pellet-Rostaing, F. Liger, M. Lemaire, R. Buchet and Y. Wu, *Bioorg. Med. Chem.*, 2009, **17**, 7290-7300; (d) C. R. Sheen, P. Kuss, S.

Narisawa, M. C. Yadav, J. Nigro, W. Wang, T. N. Chlea, E. Sergienko, K. Kapoor, M. R. Jackson, M. F. Hoylaerts, A. B. Pinkerton, W. C. O'Neill and J. L. Millán, *J. Bone Miner. Res*., 2015, **30**, 824-836.

11. L. Fishman, H. Miyayama, S. G. Driscoll and W. H. Fishman, *Cancer Res*., 1976, **36**, 2268-2273.

12. W. H. Fishman, N. K. Ghosh, N. R. Inglis and S. Green, *Enzymologia,* 1968, **34**, 317-321.

13. W. H. Fishman, N. R. Inglis, S. Green, C. L. Anstiss, N. K. Gosh, A. E. Reif, R. Rustigian, M. J. Krant and L. L. Stolbach, *Nature*, 1968, **219**, 697-699.

14. C. M. Povinelli and B. J. Knoll, *Placenta* 1991, **12**, 663-668.

15. B. Wahren, P. A. Holmgren and T. Stigbrand, *Int. J. Cancer*, 1979, **24**, 749-753.

16. B. Wahren, J. Hinkula, T. Stigbrand, A. Jeppsson, L. Andersson, P. L. Esposti, F. Edsmyr and J. L. Millán, *Int. J. Cancer*, 1986, **37**, 595-600.

17. K. A. Smans, M. B. Ingvarsson, P. Lindgren, S. Canevari, H. Walt, T. Stigbrand, T. Bäckström and J. L. Millán, *Int. J. Cancer*, 1999, **83**, 270-277.

18. C. E. Ovitt, A. W. Strauss, D. H. Alpers, J. Y. Chou and I. Boime, *Proc. Natl. Acad. Sci. U.S.A*., 1986, **83**, 3781-3785.

19. Kozlenkov, M. F. Hoylaerts, T. Ny, M.-H. Le Du and J. L. Millán, *J. Bone Miner. Res*., 2004, **19**, 1862-1872.

20. R. J. Ardecky, E. V. Bobkova, T. Kiffer-Moreira, B. Brown, S. Ganji, J. Zou, I. Pass, S. Narisawa, F. G. Iano, C. Rosenstein, A. Cheltsov, J. Rascon, M. Hedrick, C. Gaslor, A. Forster, S. Shi, R. Dahl, S. Vasile, Y. Su, E. Sergienko, T. C. Chung, J. Kaunitz, M. F. Hoylaerts, A. B. Pinkerton and J. L. Millán, *Bioorg. Med. Chem. Lett*., 2014, **24**(3), 1000-10004.

21. S. Andrews, S. J. Burgess, D. Skaalrud, J. X. Kelly and D. H. Peyton, *J. Med. Chem.*, 2010, **53**, 916-919.

22. (a) R. S. Upadhayaya, J. K. Vandavasi, R. A. Kardile, S. V. Lahore, S. S. Dixit, H. S. Deokar, P. D. Shinde, M. P. Sarmah and J. Chattopadhyaya, *Eur. J. Med. Chem.*, 2010, **45**, 1854-1867; (b) S. Eswaran, A. V. Adhikari and R. A. Kumar, *Eur. J. Med. Chem.*, 2010, **45**, 957-966; (c) C. L. Yang, C. H. Tseng, Y. L. Chen, C. M. Lu, C. L. Kao, H. Y. Tseng, M. H. Wu and C. C. Tzeng, *Eur. J. Med. Chem.*, 2010, **45**, 602-607.

23. (a) C. H. Tseng, C. C. Tzeng, C. L. Yang, P. J. Lu, H. L. Chen, H. Y. Li, Y. C. Chuang, C. N. Yang and Y. L. Chen, *J. Med. Chem.*, 2010, **53**, 6164-6179; (b) C. H. Tseng, Y. L. Chen, C. L. Yang, C. M. Cheng, C. H. Han and C. C. Tzeng, *Bioorg. Med. Chem.*, 2012, **20**, 4397-4404; (c) C. H. Tseng, Y. L. Chen, C. Y. Hsu, T. C. Chen, C. M. Cheng, H. C. Tso, Y. J. Lu and C. C. Tzeng, *Eur. J. Med. Chem.*, 2013, **59**, 274-282.

24. K. Kaur, M. Jain, R. P. Reddy and R. Jain, *Eur. J. Med. Chem.*, 2010, **45**, 3245-3264.

25. (a) N. Ahmed, K. G. Brahmbhatt, S. Sabde, D. Mitra, I. P. Singh and K. K. Bhutani, *Bioorg. Med. Chem.*, 2010, **18**, 2872-2879; (b) H. K. Peng, C. K. Lin, S. Y. Yang, C. K. Tseng, C. C. Tzeng, J. C. Lee and S. C. Yang, *Bioorg. Med. Chem. Lett.*, 2012, **22**, 1107-1110.

26. (a) P. Labrie, S. P. Maddaford, J. Lacroix, C. Catalano, D. K. Lee, S. Rakhit and R. C. Gaudreault, *Bioorg. Med. Chem.*, 2007, **15**, 3854-3868; (b) M. Naito, Y. Matsuba, S. Sato, H. Hirata and T. Tsuruo, *Clin. Cancer Res.*, 2002, **8**, 582-588.

27. X. Ji, H. Huang, Y. Li, H. Chen and H. Jiang, *Angew. Chem. Int. Ed.*, 2012, **51**, 7292-7296.

28. M. al-Rashida, R. Raza, G. Abbas, M. S. Shah, G. E. Kostakis, J. Lecka, J. Sévigny, M. Muddassar, C. Papatriantafyllopoulou and J. Iqbal, *Eur. J. Med. Chem.*, 2013, **66**, 438-449;

(b) M. al-Rashida, S. A. Ejaz, S. Ali, A. Shaukat, M. Hamayoun, M. Ahmed and J. Iqbal, *Bioorg. Med. Chem.*, 2015, **23**(10), 2435-2444.

29. P. Das, X. Deng, L. Zhang, M. G. Roth, B. M. A. Fontoura, M. A. Phillips and J. K. De Brabander, *ACS Med. Chem. Lett.*, 2013, **4**, 517-521.

30. S. Narisawa, D. Harmey, M. C. Yadav, W. C. O'Neill, M. F. Hoylaerts and J. L. Millán. *J. Bone Miner. Res.*, 2007, **22**, 1700-1710.

31. W. Humphrey, A. Dalke and K. Schulten, *J. Mol. Graphics.*, 1996, **14**, 33-38.

32. S. C. Lovell, I. W. Davis, W. B. Arendall III, P. I. W. de Bakker, J. M. Word, M. G. Prisant, J. S. Richardson and D. C. Richardson, *Proteins-Structure, Funct. Genet.*, 2003, **50**, 437-450.

33. K. Chen, K. Wang, A. M. Kirichian, A. F. Al Aowad, L. K. Iyer, S. J. Adelstei and A. I. Kassis, *Mol. Cancer Ther.*, 2006, **5**(12), 3001-3013.

34. P. Llinas, E. A. Stura, A. Ménez, Z. Kiss, T. Stigbrand, J. L. Millán and M. H. Le Du, *J. Mol. Biol.*, 2005, **350**(3), 441-451.

35. F. Kukulski, S. A. Lévesque, E. G. Lavoie, J. Lecka, F. Bigonnesse, A. F. Knowles, S. C. Robson, T. L. Kirley and J. Sévigny, *Purinergic Signal.*, 2005, **1**(2), 193-204.

36. T. Kiffer-Moreira, C. R. Sheen, K. C. da Silva Gasque, M. Bolean, P. Ciancaglini, A. van Elsas, M. F. Hoylaerts and J. L. Millán, *PLoS ONE* 2014, **9**(2): e89374.

37. R. J. Ardecky, E. V. Bobkova, T. Kiffer-Moreira, B. Brown, S. Ganji, J. W. Zou, I. Pass, S. Narisawa, F. G. Iano, C. Rosenstein, A. Cheltsov, J. Rascon, M. Hedrick, C. Gasior, A. Forster, S. H. Shi, R. Dahl, S. Vasile, Y. Su, E. Sergienko, T. D. Y. Chung, J. Kaunitz, M. F. Hoylaerts, A. B. Pinkerton and J. L. Millan, *Bioorg. Med. Chem. Lett.*, 2014, **24**(3), 1000-1004.

38. M. M. Bradford, *Analyt. Biochem.*, 1976, **72**, 248-254.

39. A. Sali and T. L. *J. Mol. Biol.*, 1993, **234**(3), 779-815.

40. E. F. Pettersen, T. D. Goddard, C. C. Huang, G. S. Couch, D. M. Greenblatt, E. C. Meng and T. E. Ferrine, *J. Comput. Chem.*, 2004, **25**, 1605-1612.

41. S. F. Altschul, W. Gish, W. Miller, E. W. Myers and D. J. Lipman, *J. Mol. Biol.*, 1990, **215**(3), 403-410.

42. ACD/Chemsketch. (2014). at <www.acdlabs.com

43. J. Wang, W. Wang, P. A. Kollman and D. A. Case, *J. Mol. Graph. Model.*, 2006, **25**(2), 247-260.

44. LeadIT. (2014). at http://www.biosolveit.de/LeadIT/

45. Accelrys Software Inc., Discovery Studio Modeling Environment, Release 4.0, San Diego: Accelrys Software Inc., 2013.

46. N. Schneider, G. Lange, S. Hindle, R. Klein and M. Rarey, *J. Comput. Aided Mol. Des.*, 2013, **27**(1), 15-29.